A Novel MDD-Based BEM Model for Transient 3T Nonlinear Thermal Stresses in FGA Smart Structures

Mohamed Abdelsabour Fahmy

Abstract

The main objective of this chapter is to introduce a novel memory-dependent derivative (MDD) model based on the boundary element method (BEM) for solving transient three-temperature (3T) nonlinear thermal stress problems in functionally graded anisotropic (FGA) smart structures. The governing equations of the considered study are nonlinear and very difficult if not impossible to solve analytically. Therefore, we develop a new boundary element scheme for solving such equations. The numerical results are presented highlighting the effects of the MDD on the temperatures and nonlinear thermal stress distributions and also the effect of anisotropy on the nonlinear thermal stress distributions in FGA smart structures. The numerical results also verify the validity and accuracy of the proposed methodology. The computing performance of the proposed model has been performed using communication-avoiding Arnoldi procedure. We can conclude that the results of this chapter contribute to increase our understanding on the FGA smart structures. Consequently, the results also contribute to the further development of technological and industrial applications of FGA smart structures of various characteristics.

Keywords: boundary element method, memory-dependent derivative, three-temperature, nonlinear thermal stresses, FGA smart structures

1. Introduction

Smart materials, which are also called intelligent materials, are engineered materials that have the ability to respond to the changes that occur around them in a controlled fashion by external stimuli, such as stress, heat, light, ultraviolet, moisture, chemical compounds, mechanical strength, and electric and magnetic fields. We can simply define smart materials as materials which adapt themselves as per required condition. The history of the discovery of these materials dates back to the 1880s when Jacques and Pierre Curie noticed a phenomenon that pressure generates electrification around a number of minerals such as quartz and tourmaline, and this phenomenon is called piezoelectric effect, so the piezoelectric materials are the oldest type of smart materials, which are utilized extensively in the fabrication of various devices such as transducers, sensors, actuators, surface acoustic wave

devices, frequency control, etc. There are a lot of smart material types like piezoelectric materials, thermochromic pigments, shape memory alloys, magnetostrictive, shape memory polymers, hydrogels, electroactive polymers and bi-component fibers, etc.

Anisotropic smart structures (ASSs) are getting great attention of researchers due to their applications in textile, aerospace, mass transit, marine, automotive, computers and other electronic industries, consumer goods applications, mechanical and civil engineering, infertility treatment, micropumps, medical equipment applications, ultrasonic micromotors, microvalves and photovoltaics, rotating machinery applications, and much more [1–12].

The classical thermoelasticity (CTE) theory of Duhamel [13] and Neumann [14] has two shortcomings based on parabolic heat conduction equation of this theory: the first does not involve any elastic terms, while the second has infinite propagation speeds of thermoelastic waves. In order to overcome the first shortcoming, Biot [15] proposed the classical coupled thermoelasticity (CCTE). But CTE and CCTE have the second shortcoming. So, several generalized thermoelasticity theories have been developed to overcome the second shortcoming of CTE. Among of these theories are Lord and Shulman (LS) [16], Green and Lindsay (GL) [17], and Green and Naghdi [18, 19] theories of thermoelasticity with and without energy dissipation, dual-phase-lag thermoelasticity (DPLTE) [20, 21] and three-phase-lag thermoelasticity (TPLTE) [22]. Although thermoelastic phenomena in the majority of practical applications are adequately modeled with the classical Fourier heat conduction equation, there are an important number of problems that require consideration of nonlinear heat conduction equation. It is appropriate in these cases to apply the nonlinear generalized theory of thermoelasticity; great attention has been paid to investigate the nonlinear generalized thermoelastic problems by using numerical methods [23–34]. Fahmy [35–39] introduced the mathematical foundations of three-temperature (3T) field to thermoelasticity.

The fractional calculus is the mathematical branch that used to study the theory and applications of derivatives and integrals of arbitrary non-integer order. This branch has emerged in recent years as an effective tool for modeling and simulation of various engineering and industrial applications [40, 41]. Due to the nonlocal nature of fractional order operators, they are useful for describing the memory and hereditary properties of various materials and processes. Also, the fractional calculus has drawn wide attention from the researchers of various countries in recent years due to its applications in solid mechanics, fluid dynamics, viscoelasticity, heat conduction modeling and identification, biology, food engineering, econophysics, biophysics, biochemistry, electrochemistry, electrical engineering, finance and control theory, robotics and control theory, signal and image processing, electronics, electric circuits, wave propagation, nanotechnology, etc. [42–44].

Several mathematics researchers have contributed to the history of fractional calculus, where Euler mentioned interpolating between integral orders of a derivative in 1730. Then, Laplace defined a fractional derivative by means of an integral in 1812.

Lacroix presented the first formula for the fractional order derivative appeared in 1819, where he introduced the nth derivative of the function $y = x^m$ as follows:

$$\frac{d^n}{dx^n} = \frac{\Gamma(m+1)}{\Gamma(m-n+1)} x^{m-n} \tag{1}$$

Liouville supposed that $\frac{d^v}{dx^v}(e^{ax}) = a^v e^{ax}$ for $v > 0$ to get the following fractional order derivative:

$$\frac{d^v x^{-a}}{dx^v} = (-1)^v \frac{\Gamma(a+v)}{\Gamma(a)} x^{-a-v} \tag{2}$$

By using Cauchy's integral formula for complex valued analytical functions, Laurent defined the integration of arbitrary order $v > 0$ as

$$_c D_x^v f(x) = {}_c D_x^{m-\rho} f(x) = \frac{d^m}{dx^m} \left[\frac{1}{\Gamma(\rho)} \int_c^x (x\text{-}t)^{\rho\text{-}1} f(t) dt \right], 0 < \rho \leq 1 \tag{3}$$

where $_c D_x^v$ denotes differentiation of order v of the function f along the x-axis. Cauchy presented the following fractional order derivative:

$$f_+^{(\alpha)} = \int f(\tau) \frac{(t-\tau)^{-\alpha-1}}{\Gamma(-a)} d\tau \tag{4}$$

In 1967, the Italian mathematician Caputo presented his fractional derivative of order $\alpha > 0$ as

$$D_*^\alpha f(t) = \frac{1}{\Gamma(m-\alpha)} \int_0^t \frac{f^{(m)}(\tau)}{(t-\tau)^{\alpha+1-m}} d\tau, m-1 < \alpha < m, \quad \alpha < 0 \tag{5}$$

Diethelm [45] has suggested the Caputo derivative to be in the following form:

$$D_a^\zeta f(\tau) = \int_a^\tau K_\zeta(\tau\text{-}\xi) f^{(m)}(\xi) \, d\xi \tag{6}$$

where $f^{(m)}$ is the mth order derivative and m is an integer such that $m\text{-}1 < \zeta \leq m$

$$K_\zeta(\tau\text{-}\xi) = \frac{(\tau\text{-}\xi)^{m\text{-}\zeta\text{-}1}}{\Gamma(m\text{-}\zeta)} \tag{7}$$

Wang and Li [46] have introduced a memory-dependent derivative (MDD)

$$D_\omega^\zeta f(\tau) = \frac{1}{\omega} \int_{\tau\text{-}\omega}^\tau K_\zeta(\tau\text{-}\xi) f^{(m)}(\xi) \, d\xi \tag{8}$$

where the first-order ($\zeta = 1$) of MDD for a differentiable function $f(\tau)$ can be expressed as

$$D_\omega f(\tau) = \frac{1}{\omega} \int_{\tau\text{-}\omega}^\tau K(\tau\text{-}\xi) f'(\xi) \, d\xi \tag{9}$$

Based on several practical applications, the memory effect needs weight $0 \leq K(\tau\text{-}\xi) < 1$ for $\xi \in [\tau\text{-}\omega, \tau]$, so the MDD magnitude $D_\omega f(\tau)$ is usually smaller than $f'(\tau)$, where the time delay ($\omega > 0$) and the kernel function ($0 \leq K(\tau\text{-}\xi) \leq 1$ for $\xi \in [\tau\text{-}\xi, \tau]$) can be chosen arbitrarily on the delayed interval $[\tau\text{-}\omega, \tau]$, the practical kernel functions are 1, $[1 - (\tau\text{-}\xi)]$ and $\left[1 - \frac{\tau\text{-}\xi}{\omega}\right]^p$, $p = \frac{1}{4}, 1, 2$, etc. These functions are monotonically increasing with $K = 0$ for the past time $\tau\text{-}\xi$ and $K = 1$ for the present time τ. The main feature of MDD is that the real-time functional value depends also on the past time $[\tau\text{-}\xi\text{-}\tau[$. So, D_ω depends on the past time (nonlocal operator), while the integration does not depend on the past time (local operator).

As a special case $K(\tau\text{-}\xi) \equiv 1$, we have

$$D_\omega f(\tau) = \frac{1}{\omega} \int_{\tau-\omega}^{\tau} f'(\xi) d\xi = \frac{f(\tau) - f(\tau - \omega)}{\omega} \to f'(\tau) \qquad (10)$$

The above equation shows that the common derivative $\frac{d}{d\tau}$ is the limit of D_ω as $\omega \to 0$. That is,

$$D_\omega f(\tau) \leq \left| \frac{\partial f}{\partial \tau} \right| = \lim_{\omega \to 0} \frac{f(\tau + \omega) - f(\tau)}{\omega} \qquad (11)$$

Now, the boundary element method (BEM) [47–80] is widely adopted for solving several engineering problems due to its easy implementation. In the BEM, only the boundary of the domain needs to be discretized, so it has a major advantage over other methods requiring full domain discretization [81–87] such as finite difference method (FDM), finite element method (FEM), and finite volume method (FVM) in engineering applications. This advantage of BEM over domain methods has significant importance for modeling of nonlinear generalized thermoelastic problems which can be implemented using BEM with little cost and less input data. Previously scientists have proven that FEM covers more engineering applications than BEM which is more efficient for infinite domain problems. But currently BEM scientists have changed their thinking and vision on BEM, where the BEM researchers developed the BEM technique for solving inhomogeneous and nonlinear problems involving infinite and semi-infinite domains by using a lot of software like FastBEM and ExaFMM.

The main objective of this chapter is to introduce a novel memory-dependent derivative model for solving transient three-temperature nonlinear thermal stress problems in functionally graded anisotropic (FGA) smart structures. The governing equations of the considered model are nonlinear and very difficult if not impossible to solve analytically. Therefore, we develop a new efficient boundary element technique for solving such equations. Numerical results show the effects of MDD on the three-temperature distributions and the influence of MDD and anisotropy on the nonlinear thermal stresses of FGA smart structures. Also, numerical results demonstrate the validity and accuracy of the proposed model.

A brief summary of the chapter is as follows: Section 1 introduces the background and provides the readers with the necessary information to books and articles for a better understanding of smart material problems, memory-dependent derivative history, and their applications. Section 2 describes the physical modeling of memory-dependent derivative problems of three-temperature nonlinear thermal stresses in FGA structures. Section 3 outlines the BEM implementation for obtaining the temperature field of the considered problem. Section 4 outlines the BEM implementation for obtaining the dispacement field of the considered problem. Section 5 introduces computing performance of the proposed model. Section 6 presents the new numerical results that describe the effects of memory-dependent derivative and anisotropy on the problem's field variations. Lastly, Section 7 outlines the significant findings of this chapter.

2. Formulation of the problem

With reference to a Cartesian system (x_1, x_2, x_3) with a configuration R bounded by a closed surface S as shown in **Figure 1**.
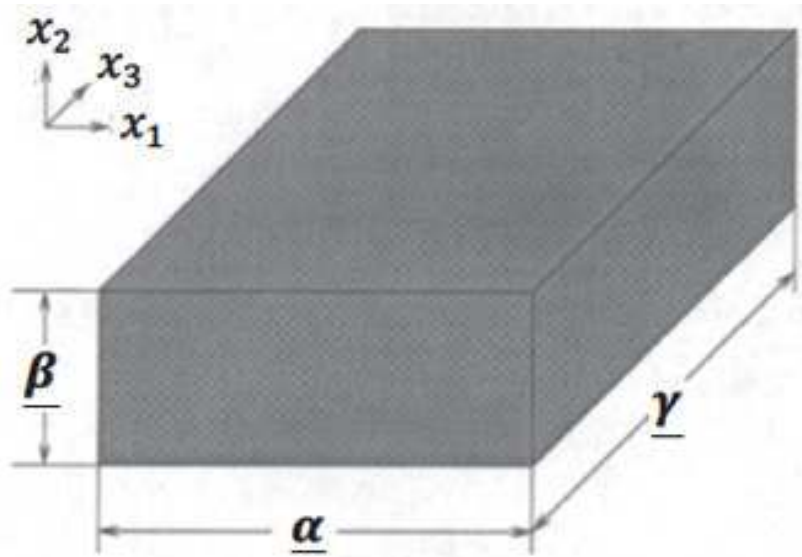
Figure 1.
Computational domain of the considered smart structure.

The governing equations for the transient three-temperature nonlinear thermal stresses problems of FGA smart structures with memory-dependent derivatives can be written as [35].

$$\sigma_{ij,j} + \rho F_i = \ddot{\pi} u_i \tag{12}$$

$$D_{i,i} = 0 \tag{13}$$

where

$$\sigma_{ij} = (x+1)^m \left[C_{ijkl} e \delta_{ij} - \beta_{ab} \left(T_\alpha - T_{\alpha 0} + \tau_1 \dot{T}_\alpha \right) \right] \tag{14}$$

$$D_i = (x+1)^m \left[e_{ijk} \varepsilon_{jk} + f_{ik} E_k \right] \varepsilon_{ij} = \frac{1}{2} \left(u_{i,j} + u_{j,i} \right), \tag{15}$$

where σ_{ij}, F_i, ε_{ij}, ε_{ijk}, u_i, and ρ are the force stress tensor, mass force vector, strain tensor, alternate tensor, displacement vector, and density, respectively, $C_{ijkl} \left(C_{ijkl} = C_{klij} = C_{jikl} \right)$ is the constant elastic moduli, e is the dilatation, $\beta_{ij} \left(\beta_{ij} = \beta_{ji} \right)$ are the stress-temperature coefficients, D_i is the electric displacement, e_{ijk} is the piezoelectric tensor, f_{ik} is the permittivity tensor, and E_k is the electric field vector.

The two-dimensional three-temperature (2D-3T) radiative heat conduction equations can be expressed as

$$c_e \frac{\partial T_e(r, \tau)}{\partial \tau} - \frac{1}{\rho} \nabla [K_e \nabla T_e(r, \tau)] = -W_{ei}(T_e - T_i) - W_{ep}(T_e - T_p) \tag{16}$$

$$c_i \frac{\partial T_i(r, \tau)}{\partial \tau} - \frac{1}{\rho} \nabla [K_i \nabla T_i(r, \tau)] = W_{ei}(T_e - T_i) \tag{17}$$

$$c_p T_p^3 \frac{\partial T_p(r, \tau)}{\partial \tau} - \frac{1}{\rho} \nabla [K_p \nabla T_p(r, \tau)] = W_{ep}(T_e - T_p) \tag{18}$$

where $e, i, \wedge p$ denote electron, ion, and phonon, respectively; (c_e, c_i, c_p), (K_e, K_i, K_p), and (T_e, T_i, T_p) are specific heat capacities, conductive coefficients,

and temperature functions, respectively; W_{ei} is the electron-ion coefficient; and W_{ep} is the electron-phonon coefficient.

3. BEM solution of temperature field

This section concerns using a boundary element method to solve the temperature model.

The above 2D-3T radiative heat conduction Eqs. (16)-(18) can be expressed in the context of nonlinear thermal stresses of FGA smart structures as in [36].

$$\nabla\left[\left(\delta_{1j}K_{\alpha} + \delta_{2j}K_{\alpha}^{*}\right)\nabla T_{\alpha}(r, \tau)\right] - \acute{W}(r, \tau) = c_{\alpha}\rho\delta_1\delta_{1j}D_{\omega_{\alpha}}T_{\alpha}(r, \tau) \tag{19}$$

which can be written in the following form:

$$L_{ab}T_{\alpha}(r, \tau) = f_{ab} \tag{20}$$

where

$$L_{ab} = \nabla\left[\left(\delta_{1j}K_{\alpha} + \delta_{2j}K_{\alpha}^{*}\right)\nabla\right] \tag{21}$$

$$f_{ab} = \acute{W}(r, \tau) + \acute{W}(r, \tau) \tag{22}$$

where

$$\acute{W}(r, \tau) = \begin{cases} \rho W_{ei}\left(T_e - T_i\right) + \rho W_{er}\left(T_e - T_p\right) + \acute{W}, \alpha = e, \delta_1 = 1 \\ -\rho W_{ei}\left(T_e - T_i\right) + \acute{W}, \qquad \alpha = i, \delta_1 = 1 \\ -\rho W_{er}\left(T_e - T_p\right) + \acute{W}, \qquad \alpha = p, \delta_1 = T_p^3 \end{cases} \tag{23}$$

$$\begin{aligned} \acute{W}(r, \tau) = F(r, \tau) &- \frac{\delta_{2j}K_{\alpha}}{\omega_{\alpha}}\int_{\tau-\omega_{\alpha}}^{\tau}K(\tau - \xi)\frac{\partial}{\partial\xi}\left(\nabla^2 T_{\alpha}(r, \tau)\right)d\xi \\ &+ \frac{\rho C_{\alpha}\delta_1\delta_{1j}}{\omega_{\alpha}}\int_{\tau-\omega_{\alpha}}^{\tau}K(\tau - \xi)\frac{\partial}{\partial\xi}\left(T_{\alpha}(r, \tau)\right)d\xi \\ &+ \frac{\rho C_{\alpha}\left(\tau_0 + \delta_{1j}\tau_2 + \delta_{2j}\right)}{\omega_{\alpha}}\int_{\tau-\omega_{\alpha}}^{\tau}K(\tau - \xi)\frac{\partial^2}{\partial\xi^2}\left(T_{\alpha}(\mathbf{r}, \tau)\right)d\xi \end{aligned} \tag{24}$$

$$F(r, \tau) = \beta_{ab}T_{\alpha 0}\left[\mathring{A}\,\delta_{1j}\acute{u}_{a,b} + \left(\tau_0 + \delta_{2j}\right)\acute{u}_{a,b}\right] \tag{25}$$

and

$$W_{ei} = \rho A_{ei}T_e^{-2/3}, W_{er} = \rho A_{er}T_e^{-1/2}, K_{\alpha} = A_{\alpha}T_{\alpha}^{5/2}, \alpha = e, i, K_p = A_p T_p^{3+B} \tag{26}$$

where $\delta_{ij}, (i, j = 1, 2), \omega_{\alpha}(0)(\alpha = e, i \wedge p)$, and $K(\tau - \xi)$ are the Kronecker delta, delay times, and kernel function, respectively.

The total energy can be expressed as

$$P = P_e + P_i + P_p, P_e = c_e T_e, P_i = c_i T_i, P_p = \frac{1}{4}c_p T_p^4 \tag{27}$$

Initial and boundary conditions can be expressed as

$$T_{\alpha}(x, y, 0) = T_{\alpha}^0(x, y) = g_1(x, \tau) \tag{28}$$

$$\mathbb{K}_\alpha \frac{\partial T_\alpha}{\partial n}\bigg|_{\Gamma_1} = 0, \alpha = e, i, \; T_p\big|_{\Gamma_1} = g_2(x, \tau) \tag{29}$$

$$\mathbb{K}_\alpha \frac{\partial T_\alpha}{\partial n}\bigg|_{\Gamma_2} = 0, \alpha = e, i, p \tag{30}$$

By using the fundamental solutions T_α^* that satisfies the following differential equation:

$$L_{ab} T_\alpha^* = f_{ab} \tag{31}$$

Now, by implementing the technique of Fahmy [35], we can write (19) as

$$CT_\alpha = \frac{D}{\mathbb{K}_\alpha} \int_O^\tau \int_S \left[T_\alpha q^* - T_\alpha^* q \right] dS d\tau + \frac{D}{\mathbb{K}_\alpha} \int_O^\tau \int_R b \, T_\alpha^* \, dR d\tau + \int_R T_\alpha^i T_\alpha^* \big|_{\tau=0} dR \tag{32}$$

which can be written in the absence of heat sources as follows:

$$CT_\alpha = \int_S \left[T_\alpha q^* - T_\alpha^* q \right] dS - \int_R \frac{\mathbb{K}_\alpha}{D} \frac{\partial T_\alpha^*}{\partial \tau} T_\alpha \, dR \tag{33}$$

In order to transform the domain integral in (33) to the boundary, we approximate the temperature time derivative as

$$\frac{\partial T_\alpha}{\partial \tau} \cong \sum_{i=1}^N f^j(r)^j a^j(\tau) \tag{34}$$

where $f^j(r)$ are known functions and $a^j(\tau)$ are unknown coefficients. We assume that $\widehat{T}_\alpha^j$ is a solution of

$$\nabla^2 \widehat{T}_\alpha^j = f^j \tag{35}$$

Then, Eq. (33) leads to the following boundary integral equation

$$CT_\alpha = \int_S \left[T_\alpha q^* - T_\alpha^* q \right] dS + \sum_{i=1}^N a^j(\tau) D^{-1} \left(C\widehat{T}_\alpha^j - \int_S \left[\widehat{T}_\alpha^j q^* - \hat{q}^j T_\alpha^* \right] dS \right) \tag{36}$$

where

$$\hat{q}^j = -\mathbb{K}_\alpha \frac{\partial \widehat{T}_\alpha^j}{\partial n} \tag{37}$$

and

$$a^j(\tau) = \sum_{i=1}^N f_{ji}^{-1} \frac{\partial T_\alpha(r_i, \tau)}{\partial \tau} \tag{38}$$

where f_{ji}^{-1} are the coefficients of F^{-1} which are defined as [58].

$$\{F\}_{ji} = f^j(r_i) \tag{39}$$

By discretizing Eq. (36) and using Eq. (38), we get [35].

$$C\dot{T}_\alpha + HT_\alpha = GQ \tag{40}$$

where Q is the heat flux vector and H and G are matrices.
The diffusion matrix can be defined as

$$C = -\left[H\widehat{T}_\alpha - G\widehat{Q}\right]F^{-1}D^{-1} \tag{41}$$

where

$$\left\{\widehat{T}\right\}_{ij} = \widehat{T}^j(x_i) \tag{42}$$

$$\left\{\widehat{Q}\right\}_{ij} = \widehat{q}^j(x_i) \tag{43}$$

To solve numerically Eq. (41), the functions T_α and q were interpolated as

$$T_\alpha = (1 - \theta)T_\alpha^m + \theta T_\alpha^{m+1} \tag{44}$$

$$q = (1 - \theta)q^m + \theta q^{m+1} \tag{45}$$

where $0 \le 0 = \frac{\tau - \tau^m}{\tau^{m+1} - \tau^m} \le 1$ determines the practical time τ of the current time step.
By time differentiation of Eq. (44), we obtain

$$\dot{T}_\alpha = \frac{dT_\alpha}{d\theta}\frac{d\theta}{d\tau} = \frac{T_\alpha^{m+1} - T_\alpha^m}{\tau^{m+1} - \tau^m} = \frac{T_\alpha^{m+1} - T_\alpha^m}{\Delta\tau^m} \tag{46}$$

By substitution from (44)–(46) into (40), we get

$$\left(\frac{C}{\Delta\tau^m} + \theta H\right)T_\alpha^{m+1} - \theta GQ^{m+1} = \left(\frac{C}{\Delta\tau^m} - (1 - \theta)H\right)T_\alpha^m + (1 - \theta)GQ^m \tag{47}$$

By considering the initial and boundary conditions, we can write the following system of equations

$$aX = b \tag{48}$$

We apply an explicit staggered algorithm to solve the system (48) and obtain the temperature in terms of the displacement field.

4. BEM solution of displacement field

By using the weighted residual method, we can write (12) and (13) in the following form:

$$\int_R \left(\sigma_{ij,j} + U_i\right)u_i^* \, dR = 0 \tag{49}$$

$$\int_R \left(D_{,i}\right)\Phi_i^* \, dR = 0 \tag{50}$$

where

$$U_i = \rho F_i - \rho \ddot{u}_i, \tag{51}$$

where u_i^* and Φ_i^* are weighting functions and u_i and Φ_i are approximate solutions.

Now, we assume the following boundary conditions:

$$u_i = \bar{u}_i \quad on \ S_1 \tag{52}$$

$$\lambda_i = \sigma_{ij} n_j = \bar{\lambda}_i \quad on \ S_2 \tag{53}$$

$$\Phi = \overline{\Phi} \quad on \ S_5 \tag{54}$$

$$Q = \frac{\partial \Phi}{\partial n} = \overline{Q} \quad on \ S_6 \tag{55}$$

By integration by parts for the first term of Eqs. (49) and (50), we have

$$-\int_R \sigma_{ij} u_{i,j}^* \, dR + \int_R U_i u_i^* \, dR = -\int_{S_2} \lambda_i u_i^* \, dS \tag{56}$$

$$-\int_R D \Phi_{,i}^* \, dR = -\int_{S_6} Q_i \Phi_i^* \, dS \tag{57}$$

Based on Huang and Liang [88], the boundary integral equation can be expressed as

$$-\int_R \sigma_{ij,j} u_i^* \, dR + \int_R U_i u_i^* \, dR - \int_R D \Phi_{,ii}^* \, dR = \int_{S_2} (\lambda_i - \bar{\lambda}_i) u_i^* \, dS + \int_{S_1} (\bar{u}_i - u_i) \lambda_i^* \, dS$$
$$+ \int_{S_6} (Q_i - \overline{Q}_i) \Phi_i^* \, dS$$
$$+ \int_{S_5} (\overline{\Phi}_i - \Phi_i) Q_i^* \, dS \tag{58}$$

By integrating by parts for the left-hand side of (58), we get

$$-\int_R \sigma_{ij} \varepsilon_{ij}^* \, dR + \int_R U_i u_i^* \, dR - \int_R D \Phi_{,ii}^* \, dR = -\int_{S_2} \bar{\lambda}_i u_i^* \, dS - \int_{S_1} \lambda_i u_i^* \, dS]$$
$$+ \int_{S_1} (\bar{u}_i - u_i) \lambda_i^* \, dS - \int_{S_6} \overline{Q}_i \Phi_i^* \, dS$$
$$- \int_{S_5} Q_i \Phi_i^* \, dS + \int_{S_5} (\overline{\Phi}_i - \Phi_i) Q_i^* \, dS \tag{59}$$

Based on Eringen [89], the elastic stress can be expressed as

$$\sigma_{ij} = \mathbb{A}_{ijkl} \, \varepsilon_{kl}, \tag{60}$$

where

$$\mathbb{A}_{ijkl} = \mathbb{A}_{klij} \tag{61}$$

Hence, Eq. (59) can be rewritten as

$$-\int_R \sigma^{ij*}\, \varepsilon_{ij}\, dR + \int_R U_i u_i^*\, dR - \int_R D\,\Phi_{i,i}^*\, dR = -\int_{S_2} \bar{\lambda}_i u_i^*\, dS - \int_{S_1} \lambda_i u_i^*\, dS$$
$$+ \int_{S_1} (\bar{u}_i - u_i)\,\lambda_i^*\, dS - \int_{S_6} \overline{Q}_i\,\Phi_i^*\, dS$$
$$- \int_{S_5} Q_i\,\Phi_i^*\, dS + \int_{S_5} (\overline{\Phi}_i - \Phi_i)\, Q_i^*\, dS$$

(62)

By integration by parts again, we obtain

$$\int_R \sigma_{ij,i}^*\, u_i dR = -\int_S u_i^*\,\lambda_i\, dS - \int_S \Phi_i^*\, Q_i\, dS + \int_S \lambda_i^*\, u_i dS + \int_S Q_i^*\,\Phi_i dS$$

(63)

The weighting functions of $U_i = \Delta^n$ and $V_i = 0$ along e_1 can be obtained as follows:

$$\sigma_{1j,j}^* + \Delta^n e_1 = 0$$

(64)

According to Dragos [90], the fundamental solution can be written as

$$u_i^* = u_{1i}^*\, e_1,\ \Phi_i^* = \Phi_{1i}^*\, e_1,\ \lambda_i^* = \lambda_{1i}^*\, e_1,\ Q_i^* = Q_{1i}^*\, e_1$$

(65)

The weighting functions of $U_i = 0$ and $V_i = \Delta^n$ along e_1 can be written as follows:

$$\sigma_{ij,j}^* = 0$$

(66)

Based on Dragos [90], the fundamental solution can be obtained analytically as

$$u_i^* = u_{1i}^{**}\, e_1,\ \Phi_i^* = \Phi_{1i}^{**}\, e_1,\ \lambda_i^* = \lambda_{1i}^{**}\, e_1,\ Q_i^* = Q_{1i}^{**}\, e_1$$

(67)

By using the weighting functions of (65) and (67) into (63), we have

$$C_{1i}^n u_i^n = -\int_S \lambda_{1i}^*\, u_i\, dS - \int_S Q_{1i}^*\,\Phi_i\, dS + \int_S u_{1i}^*\,\lambda_i\, dS + \int_S \Phi_{1i}^*\, Q_i\, dS$$

(68)

$$C_{1i}^n \omega_i^n = -\int_S \lambda_{1i}^{**}\, u_i\, dS - \int_S Q_{1i}^{**}\,\Phi_i\, dS + \int_S u_{1i}^{**}\,\lambda_i\, dS + \int_S \Phi_{1i}^{**}\, Q_i\, dS$$

(69)

Thus, we can write

$$C^n q^n = -\int_S p^*\, q\, dS + \int_S q^*\, p\, dS + \int_S d^*\,\Phi\, ds + \int_S f^*\,\frac{\partial\Phi}{\partial n}\, dS$$

(70)

where

$$C^n = \begin{bmatrix} C_{11} & C_{12} \\ C_{21} & C_{22} \end{bmatrix},\ q^* = \begin{bmatrix} u_{11}^* & u_{12}^* & 0 \\ u_{21}^* & u_{22}^* & 0 \\ u_{31}^{**} & u_{32}^{**} & 0 \end{bmatrix},\ p^* = \begin{bmatrix} \lambda_{11}^* & \lambda_{12}^* & 0 \\ \lambda_{21}^* & \lambda_{22}^* & 0 \\ \lambda_{31}^{**} & \lambda_{32}^{**} & 0 \end{bmatrix},\ q = \begin{bmatrix} u_1 \\ u_2 \\ \omega_3 \end{bmatrix},$$

$$p = \begin{bmatrix} \lambda_1 \\ \lambda \\ \mu_3 \end{bmatrix},\ d^* = \begin{bmatrix} d_1^* \\ d_2^* \\ 0 \end{bmatrix},\ f^* = \begin{bmatrix} f_1^* \\ f_2^* \\ 0 \end{bmatrix}$$

(71)

In order to solve (70) numerically, we suppose the following definitions:

$$q = \psi \, q^j, \, p = \psi \, p^j, \, \Phi = \psi_0 \, \Phi^j, \, \frac{\partial \Phi}{\partial n} = \psi_0 \left(\frac{\partial \Phi}{\partial n} \right)^j \tag{72}$$

Substituting from (72) into (70) and discretizing the boundary, we obtain

$$C^n \, q^n = \sum_{j=1}^{N_e} \left[-\int_{\Gamma_j} p^* \, \psi \, d\Gamma \right] q^j + \sum_{j=1}^{N_e} \left[\int_{\Gamma_j} q^* \, \psi \, d\Gamma \right] p^j + \sum_{j=1}^{N_e} \left[\int_{\Gamma_j} d^* \, \psi_0 \, d\Gamma \right] \Phi^j$$
$$+ \sum_{j=1}^{N_e} \left[\int_{\Gamma_j} f^* \, \psi_0 \, d\Gamma \right] \left(\frac{\partial \Phi}{\partial n} \right)^j \tag{73}$$

Equation after integration can be written as

$$C^i q^i = -\sum_{j=1}^{N_e} \hat{\mathbb{H}}^{ij} q^j + \sum_{j=1}^{N_e} \hat{\mathbb{G}}^{ij} p^j + \sum_{j=1}^{N_e} \hat{\mathbb{D}}^{ij} \Phi^i + \sum_{j=1}^{N_e} \hat{\mathbb{F}}^{ij} \left(\frac{\partial \Phi}{\partial n} \right)^j \tag{74}$$

By using the following representation:

$$\mathbb{H}^{ij} = \begin{cases} \hat{\mathbb{H}}^{ij} & \text{if } i \neq j \\ \hat{\mathbb{H}}^{ij} + C^i & \text{if } i = j \end{cases} \tag{75}$$

Thus, we can write (74) as follows:

$$\sum_{j=1}^{N_e} \mathbb{H}^{ij} q^j = \sum_{j=1}^{N_e} \hat{\mathbb{G}}^{ij} p^j + \sum_{j=1}^{N_e} \hat{\mathbb{D}}^{ij} \Phi^j + \sum_{j=1}^{N_e} \hat{\mathbb{F}}^{ij} \left(\frac{\partial \Phi}{\partial n} \right)^j \tag{76}$$

The global matrix equation for all **i** nodes can be expressed as

$$\mathbb{H}\mathbb{Q} = \mathbb{G}\mathbb{P} + \mathbb{D}\Theta + \mathbb{F}\mathbb{S} \tag{77}$$

where $\mathbb{Q}$ is the displacement vector, $\mathbb{P}$ is the traction vector, Θ is the electric potential vector, and $\mathbb{S}$ is the electric potential gradient vector.

Substituting the boundary conditions into (77), we obtain the following system of equations:

$$\mathbb{A}\mathbb{X} = \mathbb{B} \tag{78}$$

We apply an explicit staggered algorithm to solve the system (78) and obtain the temperature and displacement fields as follows:

1. From Eq. (48) we obtain the temperature field in terms of the displacement field.

2. We predict the displacement field and solve the resulted equation for the temperature field.

3. We correct the displacement field using the computed temperature field for Eq. (78).

An explicit staggered algorithm based on communication-avoiding Arnoldi as described in Hoemmen [91] is very suitable for efficient implementation in Matlab (R2019a) with the aim of specifically improving its performance for the solution of the resulting linear algebraic systems.

5. Computational performance of the problem

According to Fahmy [35], the computer performance with simulation can be computed based on account and communication process, elements underlying the hardware and functional computation. The main objective of our proposed technique during simulation process is to use the preconditioners which are efficient to improve the overall CPU utilization of the cluster, accelerate the iterative method, and reduce the input/output and the interprocessor communication costs. Also, Fahmy [35] compared the communication-avoiding Krylov methods that are based on the s-step Krylov methods such as communication-avoiding generalized minimal residual (CA-GMRES) of Saad and Schultz [92], communication-avoiding Arnoldi (CA-Arnoldi) of the Arnoldi [93] and communication-avoiding Lanczos (CA-Lanczos) of Lanczos [94], with their corresponding standard Krylov methods. CA-Arnoldi which is also called Arnoldi (s, t) algorithm is different from standard Arnoldi (s) $(s, t = 1)$, where s is the number of inner iteration steps and t is the number of outer iteration steps. According to [35], the CA-Arnoldi has numerical stability, convergence, and performance due to the implementation of algorithm shown in **Figure 2**, which is based on the QR factorization update and block classical Gram-Schmidt (block CGS) approach or block modified Gram-Schmidt (block MGS) approach where

$$V_k = [v_{sk+1}, v_{sk+2}, \ldots, v_{sk+s}] \tag{79}$$

Require: $n \times n$ matrix A and $n \times 1$ starting vector v
1: $h_0 := \|r\|_2, q_1 := v/h_0$
2: **for** $k = 0$ to $t - 1$ **do**
3:      Fix basis conversion matrix $\underline{B}_k$
4:      Compute $\acute{V}_k$ using matrix powers kernel
5:      **if** $k = 0$ **then**
6:          Compute QR factorization $\underline{V}_0 = \underline{Q}_0 R$
7:          $\underline{\Omega}_0 := \underline{Q}_0$
8:          $\underline{\mathfrak{H}}_0 := \underline{R}_0 \underline{B}_0 R_0^{-1}$
9:      **else**
10:         $\acute{\mathfrak{R}}_{k-1,k} := \underline{\Omega}_{k-1}^* \acute{V}_k$
11:         $\acute{V}_k' := \acute{V}_k - \underline{\Omega}_{k-1}\acute{\mathfrak{R}}_{k-1,k}$
12:         Compute QR factorization $\acute{V}_k' = \acute{Q}_k \acute{R}_k$
13:         Compute $\underline{\mathfrak{H}}_{k-1,k} := -\mathfrak{H}_{k-1}\mathfrak{R}_{k-1,k}R_k^{-1} + \mathfrak{R}_{k-1,k}\underline{B}_k R_k^{-1}$
14:         Compute H_k via Equation (3.21)
15:         Compute h_k via Equation (3.22)
16:         $\underline{\mathfrak{H}}_k := \begin{pmatrix} \mathfrak{H}_{k-1} & \underline{\mathfrak{H}}_{k-1,k} \\ h_{k-1}e_1 e_{s(k-1)}^T & H_k \\ 0_{1,s(k-1)} & h_k e_s^T \end{pmatrix}$
17:      **end if**
18: **end for**

Figure 2.
CA-Arnoldi iteration algorithm.

and

$$\mathcal{Q}_k = [Q_0, Q_1, \ldots, Q_{k-1}] \tag{80}$$

The generalized minimal residual (GMRES) method of Saad and Schultz [92] is a Krylov subspace method for solving nonsymmetric linear systems. The CA-GMRES algorithm is based on Arnoldi (s, t) and equivalent to standard GMRES in exact arithmetic. Also, the GMRES or CA-GMRES are convergent at the same rate for problems, but Hoemmen [91] proved that CA-GMRES algorithm shown in **Figure 3** converges for the s-step basis lengths and restart lengths used for obtaining maximum performance. Lanczos method can be considered as a special case of Arnoldi method for symmetric and real case of A or Hermitian and complex case of A. Symmetric Lanczos which is also called Lanczos is different from nonsymmetric Lanczos. We implemented a communication-avoiding version of symmetric Lanczos (CA-Lanczos) for solving symmetric positive definite (SPD) eigenvalue problems. Also, we implement CA-Lanczos iteration algorithm shown in **Figure 4**, which is also called Lanczos (s, t), where s is the s-step basis length and t is the outer iterations number before restart. This algorithm is based on using rank revealing-tall skinny QR-block Gram-Schmidt (RR-TSQR-BGS) orthogonalization method

Figure 3.
CA-GMRES iteration algorithm.

Input: $n \times n$ symmetric matrix A and $n \times 1$ starting vector r

1: $\beta_0 := \|r\|_2$, $q_1 := r/\beta_0$
2: **for** $k = 0$ to $t - 1$ **do**
3:     Fix basis conversion matrix $\underline{B}_k$
4:     Compute $\acute{\underline{V}}_k$ from q_{sk+1} and A using matrix powers kernel
5:     **if** $k = 0$ **then**
6:         $\underline{\mathfrak{B}}_0 := \underline{B}_0$
7:         Compute (via TSQR) the QR factorization $\underline{V}_0 = \underline{Q}_0 \underline{R}_0$
8:         $\underline{\Omega}_0 := \underline{Q}_k$, $\underline{\mathfrak{R}}_0 := \underline{R}_0$
9:         $T_0 := \underline{R}_0 \underline{B}_0 \underline{R}_0^{-1}$, $\underline{\mathfrak{T}}_0 := T_0$
10:     **else**
11:         $\underline{\mathfrak{B}}_k := \begin{pmatrix} \mathfrak{T}_{k-1} & 0 \cdot e_1 e_s^T \\ \beta_{sk+1} e_1 e_{s(k-1)}^T & \underline{B}_k \end{pmatrix}$
12:         $\acute{R}_{k-1,k} := \underline{Q}_{k-1}^* \acute{\underline{V}}_k$
13:         $\acute{\underline{V}}_k := \acute{\underline{V}}_k - \underline{Q}_{k-1} \acute{R}_{k-1,k}$
14:         Compute (via TSQR) the QR factorization $\acute{\underline{V}}_k = \acute{Q}_k \acute{R}_k$
15:         $\underline{\Omega}_k := [\underline{\Omega}_{k-1}, \acute{Q}_k]$
16:         Compute T_k (Eq. (4.10)) and $\beta_{s(k+1)+1}$ (Eq. (4.11))
17:         $\underline{\mathfrak{T}}_k := \begin{pmatrix} \mathfrak{T}_{k-1} & \beta_{sk+1} e_{s(k-1)} e_1^T \\ \beta_{sk+1} e_1 e_{s(k-1)}^T & T_k \\ 0_{1,s(k-1)} & \beta_{s(k+1)+1} e_s^T \end{pmatrix}$
18:     **end if**
19: **end for**

Figure 4.
CA-Lanczos iteration algorithm.

which connects between TSQR and block Gram-Schmidt, where we have been using the right-shifted basis matrix at outer iteration k as follows:

$$V_k' = [V_{sk+2}, \dots, v_{sk+s}] \tag{81}$$

and

$$V_k' = [V_k', v_{sk+s+1}] \tag{82}$$

For more details about the considered preconditioners and algorithms, we refer the interested readers to [91].

The main objective of this section is to implement an accurate and robust preconditioning technique for solving the dense nonsymmetric algebraic system of linear equations arising from the BEM. So, a communication-avoiding Arnoldi of the Arnoldi [93] has been implemented for solving the resulting linear systems in order to reduce the iteration number and CPU time. The BEM discretization is employed in 1280 quadrilateral elements, with 3964 degrees of freedom (DOF). A comparative performance of preconditioned Krylov subspace solvers (CA-Arnoldi, CA-GMRES, and CA-Lanczos) has been shown in **Table 1**, where the number of DOF is 3964 and "–" was defined as the divergence process. From the results of **Table 1**. The CA-Arnoldi, CA-GMRES, and CA-Lanczos are more cost-effective than the other Krylov subspace methods Arnoldi, GMRES, and Lanczos, respectively. Also, CA-Arnoldi, CA-GMRES, and CA-Lanczos have been compared with each other in **Table 2**. It can be seen from this table that the performance of CA-Arnoldi is superior than the other iterative methods.

Methods	Preconditioning techniques	Iterations	Residual	Time of each iterative step (s)	Time of solution
Direct methods	NO	—	—	—	9 min 50 s
Arnoldi	NO	174	7.21E–07	3.85	11 min 25 s
	JOBI	26	5.22E–07	3.86	2 min 38 s
	BJOB	22	1.34E–06	3.86	2 min 23 s
	ILU3	47	1.66E–06	3.84	4 min 2 s
	ILU5	48	1.38E–06	3.89	4 min 6 s
	DILU	48	1.53E–06	5.45	4 min 18 s
CA–Arnoldi	NO	360	6.96E–07	1.95	11 min 53 s
	JOBI	20	4.42E–07	1.96	1 min 30 s
	BJOB	20	2.30E–08	1.96	1 min 30 s
	ILU3	40	7.87E–07	1.96	2 min 11 s
	ILU5	60	1.28E–08	1.96	2 min 48 s
	DILU	60	1.59E–07	3.07	4 min 1 s
GMRES	NO	280	2.36E–08	1.90	6 min 20 s
	JOBI	40	5.01E–13	1.91	2 min 10 s
	BJOB	40	2.05E–11	1.91	2 min 10 s
	ILU3	40	4.70E–08	1.91	2 min 10 s
	ILU5	40	3.13E–08	2.60	2 min 10 s
	DILU	40	6.19E–08	3.07	2 min 48 s
CA–GMRES	NO	120	6.89E–07	3.78	7 min 57 s
	JOBI	12	1.00E–05	3.76	1 min 41 s
	BJOB	12	2.22E–06	3.76	1 min 42 s
	ILU3	26	3.63E–06	3.75	2 min 34 s
	ILU5	22	4.05E–06	3.75	2 min 20 s
	DILU	25	5.19E–06	5.93	3 min 18 s
Lanczos	NO	135	7.24E–07	3.80	8 min 41 s
	JOBI	22	4.87E–07	3.75	2 min 33 s
	BJOB	18	9.27E–07	5.18	3 min 2 s
	ILU3	42	2.41E–07	3.81	3 min 48 s
	ILU5	36	6.41E–07	3.78	3 min 18 s
	DILU	38	2.04E–07	5.00	3 min 32 s
CA–Lanczos	NO	129	1.30E–04	3.75	9 min 22 s
	JOBI	16	8.64E–07	3.76	2 min 3s
	BJOB	14	1.69E–07	3.77	2 min 0 s
	ILU3	24	9.29E–07	3.87	2 min 31 s
	ILU5	31	1.91E–07	3.90	3 min 1 s
	DILU	27	8.11E–07	5.95	3 min 31 s

Table 1.
Performances of preconditioned Krylov subspace iterative methods for DOF 3964.

Solvers		DOF				
		965	**1505**	**3380**	**3964**	**6005**
CA–Arnoldi	Residual	6.81E–12	5.38E–12	4.13E–11	4.17E–11	7.57E–11
	CPU time (s)	4.96	10.78	99.24	134.26	293.29
	Iterations	25	25	25	25	25
CA–GMRES	Residual	2.98E–12	1.90E–12	1.28E–11	1.36E–11	1.22E–11
	CPU time (s)	5.06	11.49	126.38	164.09	445.51
	Iterations	50	50	50	50	50
CA– Lanczos	Residual	7.20E–11	3.35E–11	2.72E–11	3.97E–11	8.33E–11
	CPU time (s)	5.05	11.47	139.07	180.49	514.72
	Iterations	22	26	28	30	32

Table 2.
The CPU time and the number of iterations for some communication–avoiding Krylov subspace solvers.

6. Numerical results and discussion

In order to illustrate the numerical results of this study, we consider a monoclinic graphite-epoxy as an anisotropic smart material which has the following constants [35].

The elasticity tensor is expressed as

$$
C_{pjkl} =
\begin{bmatrix}
430.1 & 130.4 & 18.2 & 0 & 0 & 201.3 \\
130.4 & 116.7 & 21.0 & 0 & 0 & 70.1 \\
18.2 & 21.0 & 73.6 & 0 & 0 & 2.4 \\
0 & 0 & 0 & 19.8 & -8.0 & 0 \\
0 & 0 & 0 & -8.0 & 29.1 & 0 \\
201.3 & 70.1 & 2.4 & 0 & 0 & 147.3
\end{bmatrix}
\text{GPa}
\tag{83}
$$

The mechanical temperature coefficient is

$$
\beta_{pj} =
\begin{bmatrix}
1.01 & 2.00 & 0 \\
2.00 & 1.48 & 0 \\
0 & 0 & 7.52
\end{bmatrix}
\cdot 10^6 \text{ N/km}^2
\tag{84}
$$

The thermal conductivity tensor is

$$
k_{pj} =
\begin{bmatrix}
5.2 & 0 & 0 \\
0 & 7.6 & 0 \\
0 & 0 & 38.3
\end{bmatrix}
\text{W/km}
\tag{85}
$$

Mass density $\rho = 7820$ kg/m^2 and heat capacity $c = 461$ J/kg k.

The technique that has been proposed in the current chapter can be applicable to a wide range of three-temperature nonlinear thermal stress problems of FGA structures. The main aim of this chapter is to assess the impact of MDD and anisotropy on the three-temperature nonlinear thermal stress distributions.

The proposed technique that has been implemented in the current study can be applicable to a wide variety of FGA smart structure problems involving three temperatures. All the physical parameters satisfy the initial and boundary conditions. The efficiency of our BEM modeling technique has been improved using an explicit staggered algorithm based on communication-avoiding Arnoldi procedure to decrease the computation time.

Figure 5 shows the variations of the three temperatures T_e, T_i and T_p with the time τ in the presence of MDD. **Figure 6** shows the variations of the three temperatures T_e, T_i and T_p with the time τ in the presence of MDD. It can be seen from **Figures 5** and **6** that the MDD has a significant effect on the temperature distributions.
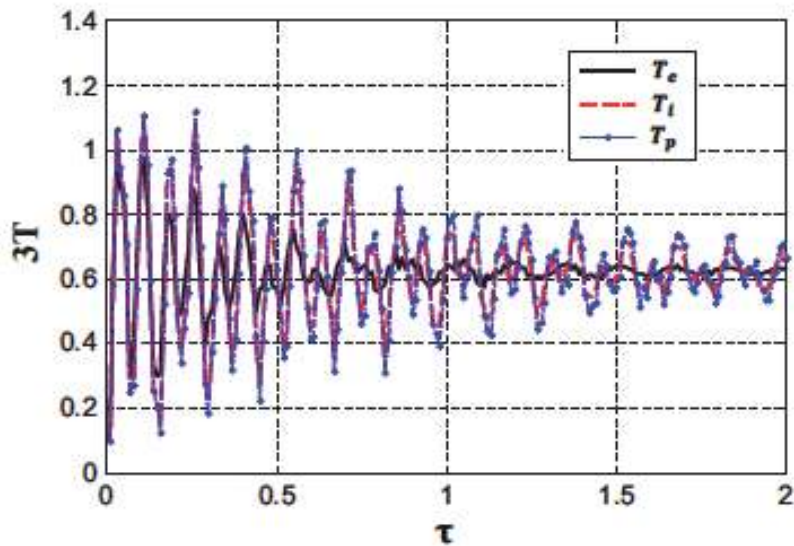
Figure 5.
Variation of the three-temperature (with memory) with time τ.
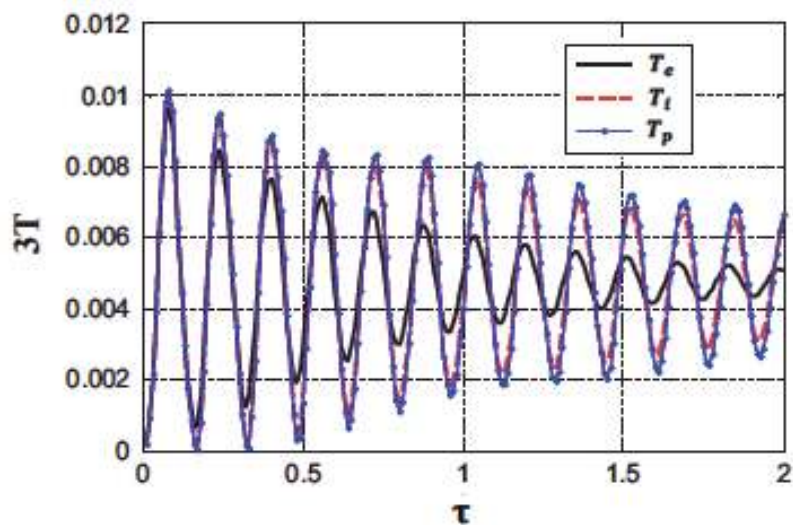
Figure 6.
Variation of the three-temperature (without memory) with time τ.

In order to study the anisotropy and MDD effects on the nonlinear thermal stresses, we assume the following four cases: A, B, C, and D, where case A denotes the nonlinear thermal stress distribution in the isotropic material without MDD effect, case B denotes the nonlinear thermal stress distribution in isotropic material with MDD effect, case C denotes the nonlinear thermal stress distribution in anisotropic material without MDD effect, and case D denotes nonlinear thermal stress distribution in anisotropic material with MDD effect.

Figures 7–9 show the variation of the nonlinear thermal stresses σ_{11}, σ_{12} and σ_{22} with the time τ. It is clear from these figures that both anisotropy and MDD have a significant influence on the nonlinear thermal stress distributions.

Since there are no available results for the considered problem in the literature. Therefore, we only considered the one-dimensional special case for the variations of the nonlinear thermal stress σ_{11} with the time τ as shown in **Figure 10**. The validity and accuracy of our proposed technique was confirmed by comparing graphically
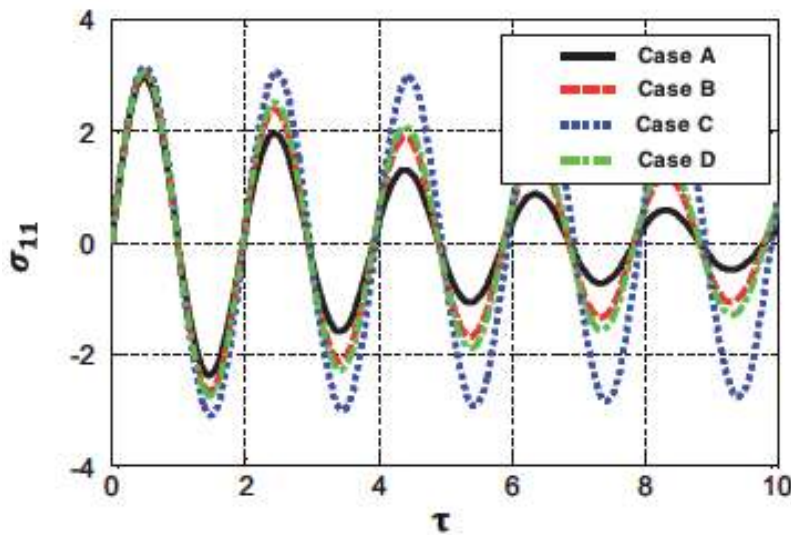

Figure 7.
Variation of the nonlinear thermal stress σ_{11} with time τ.
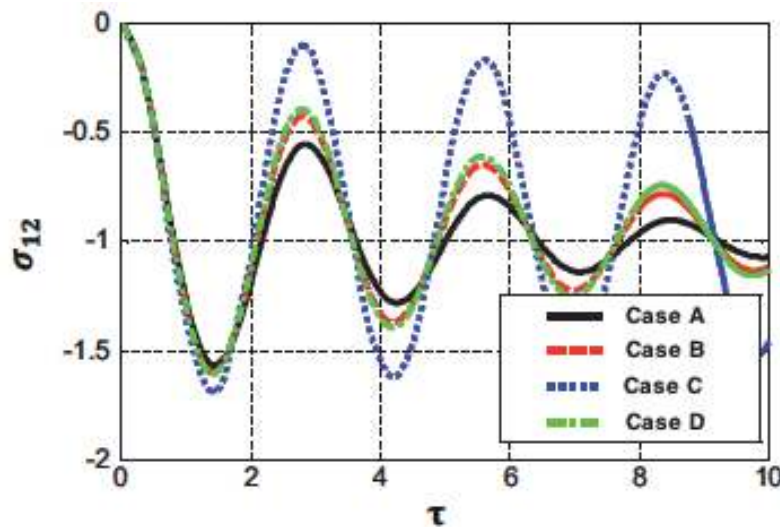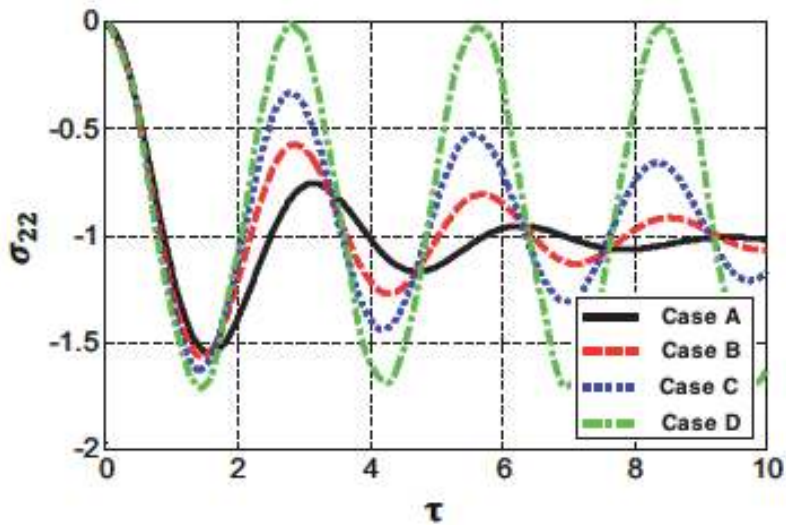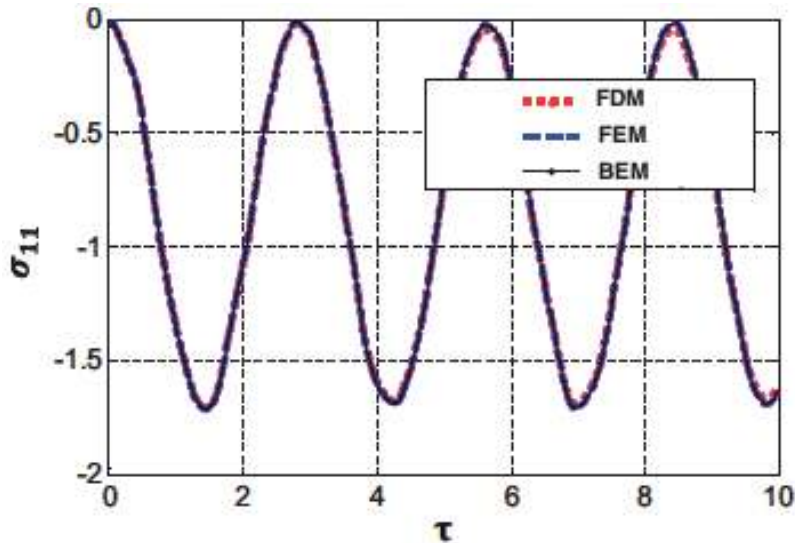

Figure 8.
Variation of the nonlinear thermal stress σ_{12} with time τ.

Figure 9.
Variation of the nonlinear thermal stress σ_{22} with time τ.

Figure 10.
Variation of the nonlinear thermal stress σ_{11} with time τ.

our BEM results with those obtained using the FDM of Pazera and Jędrysiak [95] and FEM of Xiong and Tian [96] results based on replacing one-temperature heat conduction with the total three-temperature T $(T = T_e + T_i + T_r)$ heat conduction. It can be noticed that the BEM results are found to agree very well with the FDM and FEM results.

7. Conclusion

The main aim of this chapter is to introduce a new MDD model based on BEM for obtaining the transient three-temperature nonlinear thermal stresses in FGA smart structures. The governing equations of this model are very hard to solve analytically because of nonlinearity and anisotropy. To overcome this, we propose a

new boundary element formulation for solving such equations. Since the CA kernels of the s-step Krylov methods are faster than the kernels of standard Krylov methods. Therefore, we used an explicit staggered algorithm based on CA-Arnoldi procedure to solve the resulted linear equations. The computational performance of the proposed technique has been performed using communication-avoiding Arnoldi procedure. The numerical results are presented highlighting the effects of MDD on the three-temperature distributions and the influence of MDD and anisotropy on the nonlinear thermal stresses of FGA smart structures. The numerical results also demonstrate the validity and accuracy of the proposed technique. It can be concluded from numerical results of our current general problem that all generalized and nonlinear generalized thermoelasticity theories can be combined with the three-temperature radiative heat conduction to describe the deformation of FGA smart structures in the context of memory-dependent derivatives. From the research that has been performed, it is possible to conclude that the proposed BEM technique is effective and stable for transient three-temperature thermal stress problems in FGA smart structures.

The numerical results for our complex and general problem can provide data references for computer scientists and engineers, geotechnical and geothermal engineers, designers of new materials, and researchers in material science as well as for those working on the development of anisotropic smart structures. In the application of three-temperature theories in advanced manufacturing technologies, with the development of soft machines and robotics in biomedical engineering and advanced manufacturing, transient thermal stresses will be encountered more often where three-temperature radiative heat conduction will turn out to be the best choice for thermomechanical analysis in the design and analysis of advanced smart materials and structures.

Author details

Mohamed Abdelsabour Fahmy
Faculty of Computers and Informatics, Suez Canal University, Ismailia, Egypt

*Address all correspondence to: mohamed_fahmy@ci.suez.edu.eg

IntechOpen

References

[1] Fahmy MA. A time-stepping DRBEM for 3D anisotropic functionally graded piezoelectric structures under the influence of gravitational waves. In: Proceedings of the 1st GeoMEast International Congress and Exhibition (GeoMEast 2017); 15–19 July 2017; Sharm El Sheikh, Egypt. Facing the Challenges in Structural Engineering, Sustainable Civil Infrastructures. 2017. pp. 350-365

[2] Fahmy MA. 3D DRBEM modeling for rotating initially stressed anisotropic functionally graded piezoelectric plates. In: Proceedings of the 7th European Congress on Computational Methods in Applied Sciences and Engineering (ECCOMAS 2016); 5–10 June 2016; Crete Island, Greece. pp. 7640-7658

[3] Fahmy MA. Boundary element solution of 2D coupled problem in anisotropic piezoelectric FGM plates. In: Proceedings of the 6th International Conference on Computational Methods for Coupled Problems in Science and Engineering (Coupled Problems 2015); 18–20 May 2015; Venice, Italy. 2015. pp. 382-391

[4] Fahmy MA. The DRBEM solution of the generalized magneto-thermo-viscoelastic problems in 3D anisotropic functionally graded solids. In: Proceedings of the 5th International Conference on Coupled Problems in Science and Engineering (Coupled Problems 2013); 17–19 June 2013; Ibiza, Spain. 2013. pp. 862-872

[5] Fahmy MA. A computerized boundary element model for simulation and optimization of fractional-order three temperatures nonlinear generalized piezothermoelastic problems based on genetic algorithm. In: AIP Conference Proceedings 2138 of Innovation and Analytics Conference and Exhibition (IACE 2019); 25–28 March 2019; Sintok, Malaysia. 2019. p. 030015

[6] Huang R, Zheng SJ, Liu ZS, Ng TY. Recent advances of the constitutive models of smart materials—Hydrogels and shape memory polymers. International Journal of Applied Mechanics. 2020;**12**:2050014

[7] Fahmy MA. Shape design sensitivity and optimization of anisotropic functionally graded smart structures using bicubic B-splines DRBEM. Engineering Analysis with Boundary Elements. 2018;**87**:27-35

[8] Sigmund O, Torquato S. Design of smart composite materials using topology optimization. Smart Materials and Structures. 1999;**8**:365-379

[9] Jin B, Zhong Z. A moving mode-III crack in functionally graded piezoelectric material: Permeable problem. Mechanics Research Communications. 2002;**29**:217-224

[10] Lin S, Narita F, Shindo Y. Electroelastic analysis of a penny-shaped crack in a piezo-electric ceramic under mode I loading. Mechanics Research Communications. 2003;**30**:371-386

[11] Liu W, Ma S, Wu H. Three-dimensional analysis of functionally graded piezoelectric plate with arbitrarily distributed material properties. Journal of Wuhan University of Technology. 2014;**29**(August):712-720

[12] Stanak P. Three-dimensional meshless modelling of functionally graded piezoelectric sensor. J Mech Phys Solids Mech. 2014;**2013**:425-432

[13] Duhamel J. Some memoire sur les phenomenes thermo-mechanique. Journal de l'École Polytechnique. 1837;**15**:1-57

[14] Neumann F. Vorlesungen Uber die theorie der elasticitat. Brestau: Meyer; 1885

[15] Biot M. Thermoelasticity and irreversible thermo-dynamics. Journal of Applied Physics. 1956;**27**:249-253

[16] Lord HW, Shulman Y. A generalized dynamical theory of thermoelasticity. Journal of the Mechanics and Physics of Solids. 1967;**15**:299-309

[17] Green AE, Lindsay KA. Thermoelasticity. Journal of Elasticity. 1972;**2**:1-7

[18] Green AE, Naghdi PM. On undamped heat waves in an elastic solid. Journal of Thermal Stresses. 1992;**15**: 253-264

[19] Green AE, Naghdi PM. Thermoelasticity without energy dissipation. Journal of Elasticity. 1993; **31**:189-208

[20] Tzou DY. A unified field approach for heat conduction from macro to micro scales. ASME Journal of Heat Transfer. 1995;**117**:8-16

[21] Chandrasekharaiah DS. Hyperbolic thermoelasticity: A review of recent literature. Applied Mechanics Reviews. 1998;**51**:705-729

[22] Roychoudhuri SK. On a thermoelastic three-phase-lag model. Journal of Thermal Stresses. 2007;**30**: 231-238

[23] Fahmy MA. A time-stepping DRBEM for magneto-thermo-viscoelastic interactions in a rotating nonhomogeneous anisotropic solid. International Journal of Applied Mechanics. 2011;**3**:1-24

[24] Fahmy MA. A time-stepping DRBEM for the transient magneto-thermo-visco-elastic stresses in a rotating non-homogeneous anisotropic solid. Engineering Analysis with Boundary Elements. 2012;**36**:335-345

[25] Fahmy MA. Numerical modeling of transient magneto-thermo-viscoelastic waves in a rotating nonhomogeneous anisotropic solid under initial stress. International Journal of Modeling. Simulation and Scientific Computing. 2012;**3**:1250002

[26] Fahmy MA. Transient magneto-thermo-viscoelastic stresses in a rotating nonhomogeneous anisotropic solid with and without a moving heat source. Journal of Engineering Physics and Thermophysics. 2012;**85**:950-958

[27] Fahmy MA. Transient magneto-thermo-elastic stresses in an anisotropic viscoelastic solid with and without moving heat source. Numerical Heat Transfer, Part A: Applications. 2012;**61**: 547-564

[28] Fahmy MA. Transient magneto-thermoviscoelastic plane waves in a non-homogeneous anisotropic thick strip subjected to a moving heat source. Applied Mathematical Modelling. 2012; **36**:4565-4578

[29] Fahmy MA. The effect of rotation and inhomogeneity on the transient magneto-thermoviscoelastic stresses in an anisotropic solid. ASME Journal of Applied Mechanics. 2012;**79**:1015

[30] Fahmy MA. Finite difference algorithm for transient magneto-thermo-elastic stresses in a non-homogeneous solid cylinder. International Journal of Materials Engineering and Technology. 2010;**3**:87-93

[31] Fahmy MA. Boundary element algorithm for nonlinear modeling and simulation of three temperature anisotropic generalized micropolar piezothermoelasticity with memory-dependent derivative. International Journal of Applied Mechanics. 2020;**12**: 2050027

[32] Fahmy MA. Thermal stresses in a spherical shell under three thermoelastic

models using FDM. International Journal of Numerical methods and Applications. 2009;**2**:123-128

[33] Ezzat MA, El-Karamany AS, Alaa A, El-Bary AA. On dual-phase-lag thermoelasticity theory with memory-dependent derivative. Mechanics of Advanced Materials and Structures. 2017;**24**:908-916

[34] Ezzat MA, El-Karamany AS, Alaa A, El-Bary AA. Generalized thermoelasticity with memory-dependent derivatives involving two temperatures. Mechanics of Advanced Materials and Structures. 2016;**23**: 545-553

[35] Fahmy MA. A new boundary element strategy for modeling and simulation of three temperatures nonlinear generalized micropolar-magneto-thermoelastic wave propagation problems in FGA structures. Engineering Analysis with Boundary Elements. 2019;**108**: 192-200

[36] Fahmy MA. A new computerized boundary element model for three-temperature nonlinear generalized thermoelastic stresses in anisotropic circular cylindrical plate structures. In: Awrejcewicz J, Grzelczyk D, editors. Dynamical Systems Theory. London, UK: IntechOpen; 2019. pp. 1-17

[37] Fahmy MA. Boundary element model for nonlinear fractional-order heat transfer in magneto-thermoelastic FGA structures involving three temperatures. In: Ebrahimi F, editor. Mechanics of Functionally Graded Materials and Structures. IntechOpen: London, UK; 2019. pp. 1-22

[38] Fahmy MA. Boundary element mathematical modelling and boundary element numerical techniques for optimization of micropolar thermoviscoelastic problems in solid deformable bodies. In: Sivasankaran S,

Nayak PK, Günay E, editors. Mechanics of Solid Deformable Bodies. IntechOpen: London, UK; 2020. pp. 1-21

[39] Fahmy MA. Boundary element modeling and optimization based on fractional-order derivative for nonlinear generalized photo-thermoelastic stress wave propagation in three-temperature anisotropic semiconductor structures. In: Sadollah A, Sinha TS, editors. Recent Trends in Computational Intelligence. IntechOpen: London, UK; 2020. pp. 1-16

[40] Cattaneo C. Sur une forme de i'equation de la chaleur elinant le paradox d'une propagation instantanc. Comptes Rendus de l'Académie des Sciences. 1958;**247**:431-433

[41] Oldham KB, Spanier J. The Fractional Calculus: Theory and Applications of Differentiation and Integration to Arbitrary Order. Mineola: Dover Publication; 2006

[42] Soukkou A, Belhour MC, Leulmi S. Review, design, optimization and stability analysis of fractional-order PID controller. International Journal of Intelligent Systems Technologies and Applications. 2016;**8**:73-96

[43] Kilbas AA, Srivastava HM, Trujillo JJ. Theory and applications of fractional differential equations. In: Vol. 204 of North-Holland Mathematics Studies. Amsterdam, The Netherlands: Elsevier Science; 2006

[44] Sabatier J, Agrawal OP, Machado JAT, editors. Advances in Fractional Calculus: Theoretical Developments and Applications in Physics and Engineering. Dordrecht, The Netherlands: Springer; 2007

[45] Diethelm K. Generalized compound quadrature formulae for finite-part integrals. IMA Journal of Numerical Analysis. 1997;**17**:479-493

[46] Wang JL, Li HF. Surpassing the fractional derivative: Concept of the memory-dependent derivative. Computers and Mathematics with Applications. 2011;**62**:1562-1567

[47] Fahmy MA. A three-dimensional generalized magneto-thermo-viscoelastic problem of a rotating functionally graded anisotropic solids with and without energy dissipation. Numerical Heat Transfer, Part A: Applications. 2013;**63**:713-733

[48] Fahmy MA. A 2-D DRBEM for generalized magneto-thermo-viscoelastic transient response of rotating functionally graded anisotropic thick strip. International Journal of Engineering and Technology Innovation. 2013;**3**:70-85

[49] Fahmy MA, Salem AM, Metwally MS, Rashid MM. Computer implementation of the DRBEM for studying the generalized thermoelastic responses of functionally graded anisotropic rotating plates with one relaxation time. International Journal of Applied Science and Technology. 2013;**3**:130-140

[50] Fahmy MA, Salem AM, Metwally MS, Rashid MM. Computer implementation of the DRBEM for studying the classical uncoupled theory of thermoelasticity of functionally graded anisotropic rotating plates. International Journal of Engineering Research and Applications. 2013;**3**: 1146-1154

[51] Fahmy MA. A computerized DRBEM model for generalized magneto-thermo-visco-elastic stress waves in functionally graded anisotropic thin film/substrate structures. Latin American Journal of Solids and Structures. 2014;**11**:386-409

[52] Fahmy MA, Salem AM, Metwally MS, Rashid MM. Computer implementation of the DRBEM for

studying the classical coupled thermoelastic responses of functionally graded anisotropic plates. Physical Science International Journal. 2014;**4**: 674-685

[53] Fahmy MA, Salem AM, Metwally MS, Rashid MM. Computer implementation of the DRBEM for studying the generalized thermo elastic responses of functionally graded anisotropic rotating plates with two relaxation times. British Journal of Mathematics & Computer Science. 2014;**4**:1010-1026

[54] Fahmy MA. Computerized Boundary Element Solutions for Thermoelastic Problems: Applications to Functionally Graded Anisotropic Structures. Saarbrücken: LAP Lambert Academic Publishing; 2017

[55] Fahmy MA. Boundary Element Computation of Shape Sensitivity and Optimization: Applications to Functionally Graded Anisotropic Structures. Saarbrücken: LAP Lambert Academic Publishing; 2017

[56] Fahmy MA. A new computerized boundary element algorithm for cancer modeling of cardiac anisotropy on the ECG simulation. Asian Journal of Research in Computer Science. 2018;**2**: 1-10

[57] Brebbia CA, Telles JCF, Wrobel L. Boundary Element Techniques in Engineering. New York: Springer-Verlag; 1984

[58] Wrobel LC, Brebbia CA. The dual reciprocity boundary element formulation for nonlinear diffusion problems. Computer Methods in Applied Mechanics and Engineering. 1987;**65**:147-164

[59] Partridge PW, Brebbia CA. Computer implementation of the BEM dual reciprocity method for the solution of general field equations.

Communications in Applied Numerical Methods. 1990;**6**:83-92

[60] Partridge PW, Brebbia CA, Wrobel LC. The Dual Reciprocity Boundary Element Method. Southampton: Computational Mechanics Publications; 1992

[61] Gaul L, Kögl M, Wagner M. Boundary Element Methods for Engineers and Scientists. Berlin: Springer-Verlag; 2003

[62] Zirakashvili N. Solution of contact problems for half-space by boundary element methods based on singular solutions of flamant and boussinesq's problems. International Journal of Applied Mechanics. 2020;**12**:2050015

[63] Fahmy MA. Implicit-explicit time integration DRBEM for generalized magneto-thermoelasticity problems of rotating anisotropic viscoelastic functionally graded solids. Engineering Analysis with Boundary Elements. 2013; **37**:107-115

[64] Fahmy MA. Generalized magneto-thermo-viscoelastic problems of rotating functionally graded anisotropic plates by the dual reciprocity boundary element method. Journal of Thermal Stresses. 2013;**36**:1-20

[65] Fahmy MA. A 2D time domain DRBEM computer model for magneto-thermoelastic coupled wave propagation problems. International Journal of Engineering and Technology Innovation. 2014;**4**:138-151

[66] Fahmy MA, Al-Harbi SM, Al-Harbi BH. Implicit time-stepping DRBEM for design sensitivity analysis of magneto-thermo-elastic FGA structure under initial stress. American Journal of Mathematical and Computational Sciences. 2017;**2**:55-62

[67] Fahmy MA. The effect of anisotropy on the structure optimization using

golden-section search algorithm based on BEM. Journal of Advances in Mathematics and Computer Science. 2017;**25**:1-18

[68] Fahmy MA. DRBEM sensitivity analysis and shape optimization of rotating magneto-thermo-viscoelastic FGA Structures using golden-section search algorithm based on uniform bicubic B-splines. Journal of Advances in Mathematics and Computer Science. 2017;**25**:1-20

[69] Fahmy MA. A predictor-corrector time-stepping DRBEM for shape design sensitivity and optimization of multilayer FGA structures. Transylvanian Review. 2017;**XXV**: 5369-5382

[70] Fahmy MA. Shape design sensitivity and optimization for two-temperature generalized magneto-thermoelastic problems using time-domain DRBEM. Journal of Thermal Stresses. 2018;**41**: 119-138

[71] Fahmy MA. Boundary element algorithm for modeling and simulation of dual-phase lag bioheat transfer and biomechanics of anisotropic soft tissues. International Journal of Applied Mechanics. 2018;**10**:1850108

[72] Fahmy MA. Modeling and optimization of anisotropic viscoelastic porous structures using CQBEM and moving asymptotes algorithm. Arabian Journal for Science and Engineering. 2019;**44**:1671-1684

[73] Fahmy MA. Boundary element modeling and simulation of biothermomechanical behavior in anisotropic laser-induced tissue hyperthermia. Engineering Analysis with Boundary Elements. 2019;**101**: 156-164

[74] Fahmy MA, Al-Harbi SM, Al-Harbi BH, Sibih AM. A computerized boundary element algorithm for

modeling and optimization of complex magneto-thermoelastic problems in MFGA structures. Journal of Engineering Research and Reports. 2019;**3**:1-13

[75] Fahmy MA. A new LRBFCM-GBEM modeling algorithm for general solution of time fractional order dual phase lag bioheat transfer problems in functionally graded tissues. Numerical Heat Transfer, Part A: Applications. 2019;**75**:616-626

[76] Fahmy MA. Design optimization for a simulation of rotating anisotropic viscoelastic porous structures using time-domain OQBEM. Mathematics and Computers in Simulation. 2019;**66**: 193-205

[77] Fahmy MA. A new convolution variational boundary element technique for design sensitivity analysis and topology optimization of anisotropic thermo-poroelastic structures. Arab Journal of Basic and Applied Sciences. 2020;**27**:1-12

[78] Fahmy MA. Thermoelastic stresses in a rotating non-homogeneous anisotropic body. Numerical Heat Transfer, Part A: Applications. 2008;**53**: 1001-1011

[79] Abd-Alla AM, Fahmy MA, El-Shahat TM. Magneto-thermo-elastic problem of a rotating non-homogeneous anisotropic solid cylinder. Archives of Applied Mechanics. 2008;**78**:135-148

[80] Fahmy MA, El-Shahat TM. The effect of initial stress and inhomogeneity on the thermoelastic stresses in a rotating anisotropic solid. Archives of Applied Mechanics. 2008; **78**:431-442

[81] Soliman AH, Fahmy MA. Range of applying the boundary condition at fluid/porous interface and evaluation of Beavers and Joseph's slip coefficient using finite element method. Computation. 2020;**8**:14

[82] Eskandari AH, Baghani M, Sohrabpour S. A time-dependent finite element formulation for thick shape memory polymer beams considering shear effects. International Journal of Applied Mechanics. 2019;**10**:1850043

[83] Othman MIA, Khan A, Jahangir R, Jahangir A. Analysis on plane waves through magneto-thermoelastic microstretch rotating medium with temperature dependent elastic properties. Applied Mathematical Modelling. 2019;**65**:535-548

[84] El-Naggar AM, Abd-Alla AM, Fahmy MA, Ahmed SM. Thermal stresses in a rotating non-homogeneous orthotropic hollow cylinder. Heat and Mass Transfer. 2002;**39**:41-46

[85] El-Naggar AM, Abd-Alla AM, Fahmy MA. The propagation of thermal stresses in an infinite elastic slab. Applied Mathematics and Computation. 2003;**12**:220-226

[86] Abd-Alla AM, El-Naggar AM, Fahmy MA. Magneto-thermoelastic problem in non-homogeneous isotropic cylinder. Heat and Mass Transfer. 2003; **39**:625-629

[87] Hu Q, Zhao L. Domain decomposition preconditioners for the system generated by discontinuous Galerkin discretization of 2D-3T heat conduction equations. Communications in Computational Physics. 2017;**22**: 1069-1100

[88] Huang FY, Liang KZ. Boundary element method for micropolar thermoelasticity. Engineering Analysis with Boundary Elements. 1996;**17**:19-26

[89] Eringen AC. Theory of micropolar elasticity. In: Liebowitz H, editor. Fracture. New York: Academic Press; 1968

[90] Dragos L. Fundamental solutions in micropolar elasticity. International Journal of Engineering Science. 1984;**22**: 265-275

[91] Hoemmen M. Communication-Avoiding Krylov Subspace Methods. Berkeley: University of California; 2010

[92] Saad Y, Schultz MH. GMRES: A generalized minimal residual algorithm for solving nonsymmetric linear systems. SIAM Journal on Scientific and Statistical Computing. 1986;**7**:856-869

[93] Arnoldi WE. The principle of minimized iterations in the solution of the matrix eigenvalue problem. Quarterly of Applied Mathematics. 1951; **9**:17-29

[94] Lanczos C. An iteration method for the solution of the eigenvalue problem of linear differential and integral operators. Journal of Research of the National Bureau of Standards. 1950;**45**: 255-282

[95] Pazera E, Jędrysiak J. Effect of microstructure in thermoelasticity problems of functionally graded laminates. Composite Structures. 2018; **202**:296-303

[96] Xiong QL, Tian XG. Generalized magneto-thermo-microstretch response during thermal shock. Latin American Journal of Solids and Structures. 2015; **12**:2562-2580